Research Square

Preprints are preliminary reports that have not undergone peer review.
They should not be considered conclusive, used to inform clinical practice,
or referenced by the media as validated information.

Amine-Functionalized Lignin as an Eco-Friendly Antioxidant for Rubber Compounds

June-Young Chung
Sungkyunkwan University
Uiseok Hwang
Sungkyunkwan University
Junyoung Kim
Sungkyunkwan University
Na-Yeon Kim
Sungkyunkwan University
Jeonghyeon Nam
Sungkyunkwan University
Jinho Jung
Sungkyunkwan University
Sung-Hoon Kim
Sungkyunkwan University
Jung Keun Cho
Sungkyunkwan University
Bumhee Lee
Sungkyunkwan University
In-Kyung Park
Sungkyunkwan University
Jonghwan Suhr
Sungkyunkwan University
Jae-Do Nam (jdnam@skku.edu)
Sungkyunkwan University

Research Article

Keywords: lignin, amination reaction, thermal stability, ozone resistance, fatigue resistance

Posted Date: September 29th, 2022

DOI: https://doi.org/10.21203/rs.3.rs-2087568/v1

License: This work is licensed under a Creative Commons Attribution 4.0 International License.
Read Full License

Abstract

Although the typical antioxidant, N-(1,3-dimethylbutyl)-N'-phenyl-p-phenylenediamine (6PPD), ensures high durability and long lifespan for rubber compounds, it generates a highly toxic quinone in water, causing a serious environmental pollution. Herein, as an alternative material of 6PPD, we newly introduce eco-friendly amine-functionalized lignin (AL) to be incorporated in rubber, which can provide excellent combinatorial anti-aging properties of thermal stability and ozone/fatigue resistances through radical scavenging effect. The heterolytic ring-opening reaction of AL and sulfur can accelerate curing and improve crosslink density by 28% (ν, 4.107×10^{-4} mol/cm^3), consequently reducing ozone vulnerable areas of the matrix, and further improving aging resistance. Notably, AL allows its rubber compound to exhibit superior anti-ozone performance after ozone aging, with the arithmetic surface roughness (Sa) of 2.077 μm, which should be compared to that of 6PPD (4.737 μm). The developed chemically modified lignin and the methodology have enormous potential as a promising additive for the future eco-friendly rubber compounds.

Highlights

- The eco-friendly lignin-based antioxidant was prepared through chemical modification of amination reaction.
- Primary and secondary amine groups of amine-based lignin were participated in curing to increase the crosslink density of rubber matrix.
- Amine-functionalized lignin incorporated rubber compound had excellent resistance of thermal, ozone, and fatigue.

1 Introduction

Elastomers and rubbers play an important role in modern technologies, serving as one of the main components of tires, seals, damping systems, soft robotics, wearable electronics, and stretchable sensors [1, 2]. Raw rubber is chemically crosslinked using a vulcanization process to construct permanently shaped components that provide high toughness, excellent noise- and vibration-damping properties, and chemical/thermal stabilities. However, covalent chemical bonds in the main chains of rubber are vulnerable to ozone and oxygen radicals. The ozonation reaction breaks the double bond, causing cracks, which are fatal and decrease the lifespan of rubber. Therefore, antioxidants containing polar groups, such as amines, phenolics, phosphites, or thioesters, are generally added to scavenge active radicals [3–7].

Typically, N-(1,3-dimethylbutyl)-N'-phenyl-p-phenylenediamine (6PPD) has been widely used as an antioxidant in automotive tires, where the ozone scavenging action of 6PPD occurs through reactions involving electron transfer from the p-phenylenediamine moieties to ozone molecules [8, 9]. Moreover, during the utilization of tires, approximately 1–2% of 6PPD slowly migrates to the tire surface, staining the tire brown, and the total concentration of 6PPD decreases over the lifespan of the tire [10]. However, when 6PPD is released into the environment, it transforms into 6PPD-quinone, a terribly toxic chemical,

which is the most critical drawback of utilizing 6PPD as the antioxidant. Specifically, tire wear particles, which are produced when tires roll over the road surface, are also released into the aquatic environment through surface runoff and storm water. Finally, these particles react with water to form 6PPD-quinone, which has been reported to have caused the death of 40¬–90% of salmon returning to spawn [11, 12].

In light of these issues, eco-friendly antioxidants have drawn considerable attention; one example is softwood kraft lignin (KL), a promising renewable and the most abundant feedstock of polyaromatic material sources [13]. Three monolignol precursors, viz., p-coumaryl, coniferyl, and sinapyl alcohol, are recognized in the lignin structure in the form of p-hydroxyphenyl (H), guaiacyl (G), and syringyl (S) units, respectively. Lignin molecules possess high contents of various functional groups including phenolics, alcoholic hydroxyl groups, carboxyls, carbonyls, etc., where the phenylpropanoic structures act as a radical scavenger [14, 15]. However, the typical lignin-based materials are not adequate as an alternative to the 6PPD in rubber compounds for their poor anti-aging performance [16, 17]. Moreover, when lignin is incorporated in rubber, the curing time is delayed owing to the scavenging of sulfur radicals and poor compatibility between the hydrophobic rubber and polar and/or hydrophilic lignin particles [13]. The low compatibility may not only result in degraded mechanical properties stemming from the poor interfacial adhesion between the filler and rubber matrix but can also cause the exudation of the filler onto the rubber composite surface when utilized in a dynamic environment (e.g., vehicle tire) [18–21].

In this context, amine-functionalized lignin (AL) can be a promising candidate for overcoming the drawbacks of lignin. The aliphatic amine functional groups grafted onto a lignin surface are known as one of the most effective groups for removing ozone and free radicals [22, 23]. Therefore, the AL may impart significantly enhanced aging resistance to rubber compounds compared to that of KL through its radical-scavenging effect [24, 25]. Furthermore, amine-based antioxidants have been reported to open the octatomic rings of S8 through direct nucleophilic attack, thus accelerating the vulcanization of rubber and generating more active sulfonating agents for rubber curing [26–28]. This reaction offers the possibility of the antioxidant to participate in the vulcanization reaction with a mechanism similar to that of the accelerator, and it can improve the compatibility of the antioxidant with rubber by maintaining chemical bonds with the rubber chains even after the reaction is completed.

Herein, we propose a novel eco-friendly antioxidant based on the amination reaction of KL involving the grafting of amine groups onto its surface. KL with highly reactive G and S units was used to increase the number of amine groups, which was then analyzed in a quantitative manner. We demonstrated that AL participated in the crosslinking of rubber, as evidenced by the changes in the rheological and mechanical properties such as the tensile strength, elongation, modulus, and hardness of the AL containing rubber compounds. Furthermore, we thoroughly investigated the combinatorial anti-aging properties of thermal stability and ozone/fatigue resistances of the rubber compounds incorporated with three different types of antioxidants, i.e., 6PPD, KL, and AL particles.

2 Experimental

2.1 Materials

Natural rubber (NR) was obtained from Jungwoo Co., Ltd. (Korea). Soft wood KL (lignin and ash content of ~ 97.1 and 1.6 wt.%, respectively) was supplied by Domtar Corporation (North Carolina, USA). It is a brown fine powder (elemental composition: carbon = 62.8 wt.%, hydrogen = 5.0 wt.%, oxygen = 28.1 wt.%, and sulfur = 3.6 wt.%) with a bulk density of 348 kg/m3, number-average molecular weight (M_n) of 913 g/mol, weight average molecular weight (M_w) of 1,323 g/mol, and polydispersity of 1.45, according to the specification of the manufacturer. Diethylenetriamine (DETA) and formaldehyde were obtained from Sigma-Aldrich (USA). Butadiene rubber (BR), 6PPD, naphthenic-based oil (rubber processing oil), carbon black (N330), zinc oxide, stearic acid, sulfur, N-(cyclohexylthio) phthalimide (CTP), and N-(1,1-dimethylethyl)-2-benzothiazolesulfenamide (TBBS) were purchased from Pyung Hwa Co., Ltd. (Korea).

2.2 Amine-functionalization reaction of lignin

DETA (778 mL) and formaldehyde (265 mL) were dissolved in 4 L of deionized (DI) water in a 10 L reactor, and then, a 10 M NaOH solution was added slowly. After stirring for 10 min, KL (1.2 kg) was added to the DETA/formaldehyde solution, and the resulting mixture was allowed to react for 9 h at 60°C under stirring and bubbling of nitrogen gas. The reacted mixture was then cooled to ambient temperature, and the pH was adjusted to 7 using 3 M HCl. In order to remove unreacted species, the resulting slurry was washed repeatedly with deionized water through centrifugation at 3000 rpm until the pH of the solution became < 7. Finally, a light brown powder was obtained after drying overnight under vacuum at 65°C. The synthesis scheme is presented in Fig. 1a

2.3 Preparation of natural/butadiene rubber compounds (NB)

NR and BR were combined and masticated at the beginning of mixing using an internal mixer kneading machine (Namyang, Korea), followed by the addition of processing oil, N330, zinc oxide, stearic acid, and various types of antioxidants (i.e., 6PPD, KL, and AL). The temperature and rotor speed were maintained at 80°C and 40 rpm, respectively. Then, the resulting rubber compounds were mixed with sulfur, CTP, and TBBS using an 8-inch two-roll mill (Intech System, TX-2143CR, Korea) at room temperature (RT). The rotor speed ratio of the rolls was maintained at 1:1.2 throughout the mixing cycle. Finally, composite specimens were prepared by compression molding at 160°C and 20 MPa. The all-NB compounds were named after their type and content of antioxidant, for example, NB compounds with 6PPD, KL, and AL are termed NB/6P, NB/KL, and NB/AL, respectively, while NB added of 1, 2, and 4 phr of AL particles are termed NB/AL-1, NB/AL-2, and NB/AL-4.

2.4 Characterization

The size and morphology of the samples were analyzed by field-emission scanning electron microscopy (FE-SEM, JEOL JSM 7401F, Japan). The chemical groups and surface characteristics were investigated using Fourier-transform infrared (FT-IR) spectroscopy (Bruker, IFS-66/S, Germany) and X-ray

photoelectron spectroscopy (XPS) (Thermo ESCALAB 250, USA), respectively. Thermogravimetric analysis (TGA) and derivative thermogravimetry (DTG) (TG/DTA 7300, Hitachi, Japan) were performed in nitrogen from room temperature to 700°C at a heating rate of 10°C/min.

2.5 Rheological and mechanical properties characterization

The curing characteristics of the fractured surfaces of rubber compounds were monitored using a rheometer (MDR, Daekyung Teck & Tester, Korea) at 160°C for 20 min under an oscillation angle of 1°. Tensile tests were performed according to ASTM D412 using dumbbell-shaped specimens (type-3, thickness = 2 mm) of the NB compounds with an automatic universal testing machine (UTM) (Daekung Teck & Tester, Korea) at a speed of 500 mm/min. The tensile strength, elongation at break, and 50% modulus were measured on four specimens, and the average values were used. The hardness of the rubber compounds was measured according to ASTM D2240-15 using a durometer (A type) on five different spots of the samples (30 × 30 × 8 mm), and average values were used. The NB compounds were subjected to a swelling test to calculate the crosslink density [29]. Swelling experiments were carried out with the molded samples (50 × 30 × 2 mm) by putting them in toluene for 48 h at 25°C according to ASTM D471. The test specimens were then removed from the toluene, wiped with tissue paper to remove excess solvent from the surface, and weighed. The swelling index (*Q%*) and dissolution fraction (*s*) were then calculated as follows:

$$Q\% = \frac{W_{sw} - W_0}{W_0} \times 100\% \quad (1)$$

$$s = \frac{W_0' - W_0}{W_0'} \times 100\% \quad (2)$$

where W_{sw} and W_0' represent the weights of the samples after swelling and free from dissolved matter, respectively, and W_0 is the weight of the samples after drying in vacuum oven until the weight is constant. The swelling data were utilized to obtain the average molecular weight between cross-linking points, M_c (g/mol) by applying Flory–Rehner relation.

$$M_c = \frac{-V_s V_r^{1/3}}{[\ln(1-V_r) + V_r + \chi V_r^2]} \times 100$$

3

where V_s is the molar volume of the solvent, χ is the interaction parameter of rubbers where the χ of NB compound is 0.365, which is average χ of NR (0.39) and BR (0.34), and V_r is the volume fraction of swollen rubber, which can be obtained from the masses and densities of the rubber sample and solvent. The crosslink density (v, mol/cm^3) is given by:

$$v = \frac{\rho}{M_c}$$

where ρ is the density of rubber

2.6 Anti-aging performance measurements

To analyze the thermal aging resistance of the rubber compounds, the specimens were placed in a convection oven at 120°C for 24 h and then allowed to cool at RT for 24 h. Mechanical properties of the thermally aged specimens were evaluated using the aforementioned unaged rubber tensile test method. The ozone aging studies were conducted according to the ASTM D1149 standard in ozone test chamber at 40°C. Ozone concentration in the chamber was adjusted to 50 pphm. The tests were carried out for 72 h under 20% stretching in ozone aging test chamber. After the ozone aging test, the three-dimensional (3D) images and surface roughness parameter, including arithmetical roughness average (Sa), root mean square roughness (Sq), and maximum height (Sz) of rubber compounds were measured with a 3D laser scanning microscopy (3D LSM OLS5100, OLYMPUS, Japan). Flex fatigue (cycles of failure) was evaluated according to ASTM D4482-06.

3 Results And Discussion

Figure 1a and Scheme S1 show schematics of the amine-functionalization reaction of KL using DETA and formaldehyde. In the DETA/formaldehyde solution, formaldehyde reacted with the primary or secondary amine groups of DETA to form immonium ions, which were generated in the presence of a high electron density of carbon atoms. Subsequently, immonium ions reacted with phenolic moieties in lignin to introduce amine groups only at the ortho and/or para positions of the phenolic hydroxyl group. Thus, the H and/or G units with free phenolic hydroxyl groups were converted to C5 amine-substituted units [30, 31]. The presence of amine groups caused the dark brown KL powder to turn light brown following the reaction. FE-SEM images of the KL and AL particles are shown in Fig. 1b and 1c, respectively, where the morphologies appear to be similar. The corresponding EDS elemental mapping images of KL (Fig. S1) and AL (Fig. 1d and S2) clearly compare the distribution of the elements, indicating the grafting of amine groups on the AL particles with nitrogen after the amination reaction. The atomic percentage of nitrogen increased from 0.89 to 13.37% after the reaction, whereas the carbon content decreased from 79.94 to 68.97%.

Spectral analysis data (FT-IR spectra, XPS spectra, and TGA/DTA curves) of the KL and AL particles are shown in Fig. 2. The FT-IR spectra were used to investigate the changes in the chemical structure of the particles after the modification process (Fig. 2a). The band located at ~ 3404 cm^{-1} for KL was assigned to the hydroxyl groups in the aliphatic and phenolic structures of lignin while the relatively broader band in the 3500–3300 cm^{-1} range of AL was attributed to N–H stretching vibrations of the primary and secondary amines grafted by the amination reaction [32]. The peaks at 2928 and 2840 cm^{-1} were originated from the C–H asymmetrical and symmetrical stretching vibrations of the methyl and methylene groups, respectively [33], and their peak intensities increased significantly after modification. This suggests the successful introduction of the molecular chains containing numerous methyl and

methylene groups during the amination reaction. Because the reaction occurred at the aromatic moieties of lignin, the intensity of the peaks corresponding to the C–H vibrations of the aromatic skeleton (1603, 1506, and 812 cm^{-1}), aromatic in-plane bending (1146 and 1025 cm^{-1}), and C–O vibrations of guaiacyl ring (1269 cm^{-1}) of lignin decreased markedly in the spectrum of AL [33, 34]. Furthermore, a new peak appeared at 1640 and the intensity of the peak at 1357 cm^{-1} was increased for AL, which arose from the N–H bending and C–N stretching vibrations of the $–NH_2$ structure, respectively, implying that the amine groups were successfully grafted onto the lignin structure [35, 36].

The change in the chemical composition of lignin particle surface after the reaction was further confirmed by XPS (Fig. 2b–2d). When the spectra of KL and AL were compared, the C1s and O1s binding energies of KL and AL particles were found to be 285.1 and 533.1 eV, respectively, and a new N1s peak was observed at 399.5 eV for AL, as shown in Fig. 2b. Notably, AL had a high N/C ratio (0.18), which is about 18 times higher than that of KL (0.01). In addition, a large increase in the C/O area ratio from 3.32 (KL) to 3.67 (AL) was observed, indicating that alkyl amine groups were introduced into the carbon chains of AL, leading to a higher carbon content and lower oxygen content. For more detail, in the N1s core-level spectra of AL (Fig. 2c), primary ($–NH_2$) and secondary amine groups (–NH) were detected on the AL surface, indicating that the terminal primary amine of DETA and lignin reacted to form a chemical structure, as illustrated in the inset of Fig. 2b. As shown in Fig. 2d, the deconvoluted C1s spectra of KL and AL show peaks at 284.5, 284.8, and 286.2 eV corresponding to the carbon atoms located in aromatic rings, sp_2 and sp_3 hybridized carbon atoms (C–C/C = C), and functional groups of lignin (C–N/C–O), respectively [37–39]. As amine groups were grafted on the AL surface mainly via the formation of C–N linkages, the area fraction of C–N/C–O increased from 31.37 to 48.51%. These changes in N1s and C1s spectra following modification suggest the presence of both primary and secondary amine groups, indicating successful grafting of amine groups on AL particles.

Figure 2e and 2f represent the TGA/DTG curves of KL and AL recorded under N_2 atmosphere. Slight weight loss and the peaks detected below 150°C in the TGA and DTG curves, respectively, were attributed to the evaporation of residual moisture because lignin usually contains water in the cell walls. In the range of 150–300°C, the low-molecular-weight lignin fragments were decomposed and evaporated (Fig. 2e). Specifically, in the DTG curves (Fig. 2F), two weight loss peaks were observed at 241°C (weight loss rate, R_{wt}: −0.56%/min) and 277°C (R_{wt}: −1.05%/min) for KL, and a single bond weight loss peak was observed at 255°C (R_{wt}: −1.18%/min) for AL, which may be ascribed to the degradation and evaporation of low molecular weight lignin fragments from aliphatic side chains [35]. In the decomposition step above 300°C, the weight loss peak of KL was observed at 391°C, while two peaks were observed at 312 and 363°C for AL, corresponding to C–C bond cleavage and demethoxylation of aromatic rings [35, 40]. The maximum weight loss rates were observed at 392°C (R_{wt}: −3.68%/min) for KL and at 364°C (R_{wt}: −2.67%/min) for AL. The lower temperature observed for AL can be attributed to the lower C–N bond energy compared to that of C–C bond [31]. In the final stage above 500°C, only a small weight loss was observed for both samples.

Figure 3a and 3b show the evolution of the rheological properties of the rubber compounds during vulcanization according to the amount of 6PPD, KL, and AL added as an antioxidant. The curing characteristics are expressed in terms of the torque value at the initial (moment of lowest, ML) and late stages (moment of highest, MH), crosslink density, as measured indirectly from the difference in torque (ΔMH = MH − ML), scorch time (ts_2), optimum curve time (tc_{90}), and cure rate index (CRI), as listed in Table S1. The comparison of the rheological results of NB/KL-2 with those of NB/6P-2 revealed two contradictory trends; the ts_2 and tc_{90} of NB/KL-2 were 4.30 and 6.98 min, respectively, which are 22 and 15% higher than those of NB/6P-2 (3.37 and 5.93 min). Furthermore, the CRI value of NB/KL-2 was 37.31 min^{-1}, which is 5% lower than that of NB/6P-2 (39.06 min^{-1}). These results indicated that lignin scavenged the activated sulfur radicals, thus interfering with the crosslinking reaction [21, 41]. The torque value of NB/KL-2 indicated that the ML, MH, and ΔMH of the compound increased, although the large number of hydroxyl groups in purified lignin particles could limit their interaction with the rubber matrix. This is possibly because the micron-sized lignin particles interfered with the movement of rubber chains, or the sulfur contained in lignin and rubber led to their cross-linking to render the composite harder [42].

A comparison between the NB/AL and NB/6P-2 in the rheological properties revealed a different trend from the NB/KL-2. The MH of NB/AL-2 was 24.40 dNm, which is 28 and 17% higher than those of NB/6P-2 (19.06 dNm) and NB/KL-2 (20.84 dNm), respectively, at the same filler content. The CRI value of NB/AL-2 was 61.35 min^{-1}, which is 57% higher than that of NB/6P-2. Furthermore, with increasing AL content for the NB/AL specimens, the torque in the whole-time range and CRI were increased. These results are presumably because the amine groups in the AL particles acted as nucleophilic activators; they not only accelerated the vulcanization reaction of rubber, but also increased the degree of crosslinking, as illustrated in Fig. 3c. A heterolytic ring-opening reaction occurred when the amine groups grafted onto the AL particles met a sulfur ring. This reaction was initiated with the nucleophilic attack of the primary and secondary amines on the sulfur ring to produce a polysulfide [43, 44], which is expected to increase the amount of polarizable sulfur in the matrix. The sulfur on the surface of AL particles could be separated from the particles allowing the rubber matrix to further vulcanized (i.e., sulfur donor) or directly reacted with the double bonds in the rubber chains to participate in the curing reaction.

The thermal aging test is a method of confirming the characteristics of rubber that is aged by heat applied from the outside or formed inside through repeated deformation, and thus significantly important factors directly related to the lifespan of rubber. Figure 4a shows the effects of thermal aging on the tensile properties of the NB compounds. The 50% modulus value of NB/KL-2 was 1.14 MPa, which is slightly higher than that of NB/6P-2 (1.06 MPa), but the tensile strength and elongation were almost the same for the two samples. This is because, although KL has low compatibility, the sulfur contained in lignin participated in the crosslinking reaction with rubber to prevent the deterioration of the physical properties of cured rubber or the amount of added lignin was not too high to degrade the mechanical properties of the rubber. On the other hand, the 50% modulus of NB/AL-1, NB/AL-2, and NB/AL-4 were 1.25, 1.36, and 1.53 MPa, respectively. All NB/AL compounds exhibited higher stress than NB/6P-2 over the entire strain range. The 50% modulus values of NB/AL compounds were higher than those of NB/6P-

2 and NB/KL-2, indicating that the amine-grafted lignin not only accelerated the curing reaction of rubber more significantly than 6PPD and KL, but also participated directly in curing to increase the crosslink density of the samples, thereby improving its mechanical properties. After the thermal aging, the modulus increased, and the tensile strength and elongation decreased for all specimens. These were due to the simultaneous occurrence of two aging processes in rubber: hardening by crosslinking and softening by chain scissioning, respectively. These interesting results mainly derived from the hybrid rubber matrix consisting of NR and BR, between which NR with bulky side groups cannot easily undergo radical recombination reactions owing to steric hindrance; it was therefore degraded by chain scissioning caused by disproportionation and hydrogen abstraction [45]. On the other hand, crosslinking dominated in BR with less-active double bonds because of the electron-withdrawing groups [46].

Figure 4b shows the degree of deterioration of the tensile properties resulting from thermal aging. The tensile strength and elongation of NB/AL-2 decreased by 36.2 and 46.9%, respectively, by a lower degree than those of NB/6P-2 and NB/KL-2. These results indicated that the AL particles imparted excellent anti-aging properties to rubber. The NB/AL compounds exhibited lesser change in tensile strength than in elongation, compared to the other samples. This is possibly because the free radical of the NB rubber chains reacted with oxygen molecules to form rubber–O• or rubber–OH, which then reacted with amine groups grafted onto the AL particles. Detailed and additional information on the variation in the tensile properties and hardness of the specimens after thermal aging was provided in Table S2, which reveals that unaged NB/AL compounds had higher hardness than the others, and that the hardness of NB/AL compounds increased by a lower degree than those of NB/6P-2 and NB/KL-2, after thermal aging.

Figure 4c and Table S3 show swelling behaviors of the rubber compounds in solvent, which exhibit the effect of antioxidants on the crosslinking of rubber. Generally, there are two main opposing forces in swelling of crosslinked polymers, i.e., solvent infiltration into the polymer network and resistance of the network to expansion [47]. NB/KL-2 exhibited higher $Q\%$ (208.3%) and lower v (3.22×10^{-4} mol/cm^3) than those of NB/6P-2 (197.9% and 3.795×10^{-4} mol/cm^3, respectively). These results can be attributed to the fact that the radical scavenging effect and micron size of lignin physically/chemically interfered with the crosslinking of rubber during the vulcanization reaction. On the other hand, the $Q\%$ and v of NB/AL-1 were 189.3% and 3.964×10^{-4} mol/cm^3, respectively, and as the content of AL particles increased, $Q\%$ decreased and v increased. It should be addressed that, at the same filler content, v of NB/AL-2 is 8 and 28% higher than those of NB/6P-2 and NB/KL-2, respectively. It is considered that the amount of activate sulfur increased during the vulcanization process because of the presence amine groups on AL particles. These results are also in good agreement with the substantially increased torque values of the NB/AL-2, compared to the NB/6P-2 and NB/KL-2 (Fig. 3).

Figure 4d shows the digital images of NB compounds immersed in a toluene after 48 h during the swelling test. It was clearly confirmed that only NB/6P-2 changed the color of the solvent to yellow. Furthermore, the s of NB/6P-2 was 10.46%, whereas those of all other samples were about 9.50% (Table S3). This is because 2 phr of 6PPD (1 wt.%), which was not chemically bound to the rubber, was almost dissolved in the toluene penetrating out of the rubber. On the other hand, lignin-incorporated samples (i.e.,

NB/KL-2 and NB/AL-2) maintained the solvent transparently without any color change. This is attributable to the polar characteristic of lignin in nature, making it difficult to be dissolved in non-polar solvents such as toluene, and even if the rubber swells providing increased interstices between the polymer chains, it may be difficult for micro-sized particles to escape to the rubber surface.

Ozone resistance is one of the critical properties in rubber compounds that resists the formation of microcracks through chemical attack to rubber, thereby suppressing deterioration of rubber performance and extending lifespan. The initiation of cracks under stretching is due to the reaction occurring between double bonds of rubber chain and ozone, i.e., ozonolysis. The rapid reaction of ozone with olefinic double bonds forms an ozonide ring, which is subsequently broken causing macroscopic surface cracks. Furthermore, ozone cracking occurs not only in surface of rubber compounds but also in interfaces between filler and matrix because ozone can penetrate faster within the rubber structure at a higher temperature.

In the case of NB/KL-2, due to the low compatibility of KL, air gaps were formed between the particles and the matrix, increasing the exposed area vulnerable to ozone. As a result, cracks were simultaneously generated both internally and externally, and the growing cracks eventually led to specimen cutting, as shown in Fig. S3. Figure 5a and 5b show the digital and optical microscope images of NB/6P-2 and NB/AL-2, respectively, after ozone aging under 20% stretching. In general, 6PPD with a relatively small molecular weight (298.38 g/mol) blooms on the surface and exerts a sufficient barrier effect against ozone attack [48, 49]. However, after ozone aging, numerous small cracks with sizes of 100–200 μm and large cracks over 1 mm were formed on the surface of NB/6P-2 due to the severe aging conditions. On the other hand, it is noteworthy that the surface of NB/AL-2 showed intermediate cracks with sizes ranging from 0.1 to 1 mm. As the AL was crosslinked with rubber and had restricted particle movement, it is considered that cracks may occur in other parts except for the part where the AL particles were dispersed near the surface. In addition, since NB/AL-2 had a small amount of unreacted double bonds of rubber chain to be attacked by ozone, micro-cracks were hardly generated on the surface.

Figure 5c and 5d show the 3D images and surface profiles of rubber surfaces using optical profilometry, which is a non-contact metrology technique for surface analysis and topographical characterization. In case of NB/6P-2, large crack with a depth of 162.05 μm and a width of 56.90 μm and small cracks of < 10 μm were detected on the surface. The surface roughness parameter values of NB/6P-2 were Sa = 4.737 μm, Sq = 13.199 μm, and Sz = 213.217 μm, respectively. In contrast, NB/AL-2 had a smaller crack (depth = 67.76 μm and width = 22.26 μm) and lower surface roughness parameter values (Sa = 2.077 μm, Sq = 4.047 μm, and Sz = 115.138 μm) than those of NB/6P-2 (Table S4). The exceptional ozone resistance of NB/AL-2 can be attributable to the reduction of the uncured area of matrix and radical scavenging performance of AL particles. These results suggest that the amination modification of lignin significantly improves the reactivity with radicals generated from ozone, imparting rubber with excellent ozone-aging resistance.

Figure 6 shows the results of predicting the fatigue life of rubber by the fracture of unaged or thermally aged specimens under repeated deformation conditions. The mechanical theory of the fatigue failure mechanism is that, in the process of fatigue, the molecular chains of rubber are broken by mechanical force, and the free radicals produced react with oxygen to induce oxidative aging, causing the fracture of molecular chains and formation of microcracks, which gradually expand with time [50, 51]. Considering this mechanism, the number of cycles was taken as a measure of the service life of the tested rubber compounds. The number of cycles to failure (Nf) of NB/6P-2 was 90,001, because 6PPD imparted excellent fatigue resistance properties by quickly reacting with the radicals of the rubber chains that were physically generated and removing them. In the case of NB/KL-2, the weak bonds between the rubber and lignin were first broken during the fatigue process, resulting in the formation of large cracks in the rubber matrix. Consequently, NB/KL-2 performed poorly (16,234 cycles) under fatigue conditions. On the other hand, the Nf of NB/AL-2 was 89,934 cycles, which is similar to that of NB/6P-2. Remarkably, after thermal aging, the NB/AL-2 (84,931 cycles) exhibited much better fatigue resistance compared to that of the NB/6P-2 (79,052 cycles). These improved fatigue resistances of NB/AL-2 were attributed to the interconnected composite structures derived from the presence of the AL particles, which were physically entangled and chemically crosslinked into the matrix and thereby effectively endured to external stress. Combined with the excellent fatigue resistance evidenced by the flex fatigue test, it can be concluded that the AL is one of the best candidate antioxidants that can be incorporated to rubber.

4 Conclusion

In this study, we successfully fabricated amine-functionalized lignin by a chemical modification method. Using an amination reaction with DETA, primary and secondary amine groups were introduced onto the surface of lignin, improving radical scavenging effect. When incorporated in rubber, the AL particles imparted superior resistance to thermal and ozone aging characteristics, comparable to those of 6PPD. The AL particles directly participated in the vulcanization reaction of rubber and promoted the activation of sulfur to increase the curing rate and crosslink density of rubber, further improving the fatigue resistance by physically and chemically bonding with rubber. By replacing 6PPD, which is considered a significant concern in aquatic pollution, the eco-friendly lignin-based antioxidant has an enormous potential to reduce environmental pollution, paving the way for the next-generation rubber industry.

Declarations

Supplementary information

The online version contains supplementary material available at

Funding

This work was supported by projects from the U.S. Air Force Office of Scientific Research/AOARD (grant numbers: FA2386-19-1-4056 and FA2386-22-1-0041). We also appreciate the instrumental and financial

support from research grants and projects supported by the National Research Foundation of Korea (NRF-2019R1A2C1005922) and the Technology Innovation Program (KEIT-20013794, MOTIE).

Author contributions

J.-Y. Chung took part in conceptualization, visualization, methodology, investigation, writing – original draft, and writing – review & editing. U. Hwang, J. Kim, and N.-Y. Kim involved in investigation and visualization. J. Nam and J. Jung took part in investigation. S.-H. Kim and J.K. Cho involved in conceptualization, investigation, and methodology. I.-K. Park and J. Suhr took part in funding acquisition. J.-D. Nam involved in conceptualization, methodology, writing – review & editing, supervision, and funding acquisition. All authors read and approved the manuscript.

Conflict of Interest

The authors declare no conflict of interest.

References

1. D. Basu, A. Das, K.W. Stöckelhuber, U. Wagenknecht, G. Heinrich. Advances in layered double hydroxide (LDH)-based elastomer composites. Prog. Polym. Sci. **39**(3), 594-626 (2014). https://doi.org/10.1016/j.progpolymsci.2013.07.011
2. X. Wei, P. Peng, F. Peng, J. Dong. Natural Polymer Eucommia Ulmoides Rubber: A Novel Material. J. Agric. Food Chem. **69**(13), 3797-821 (2021). https://doi.org/10.1021/acs.jafc.0c07560
3. G.-Y. Li, J.L. Koenig. A Review of Rubber Oxidation. Rubber Chem. Technol. **78**(2), 355-90 (2005). https://doi.org/10.5254/1.3547888
4. G.J. Lake. Ozone Cracking and Protection of Rubber. Rubber Chem. Technol. **43**(5), 1230-54 (1970). https://doi.org/10.5254/1.3547321
5. F. Cataldo. On the ozone protection of polymers having non-conjugated unsaturation. Polym. Degrad. Stab. **72**(2), 287-96 (2001). https://doi.org/10.1016/S0141-3910(01)00017-9
6. F. Cataldo, B. Faucette, S. Huang, W. Ebenezer. On the early reaction stages of ozone with N,N'-substituted p-phenylenediamines (6PPD, 77PD) and N,N',N''-substituted-1,3,5-triazine “Durazone®”: An electron spin resonance (ESR) and electronic absorption spectroscopy study. Polym. Degrad. Stab. **111**, 223-31 (2015). https://doi.org/10.1016/j.polymdegradstab.2014.11.011
7. N. Ning, Q. Ma, Y. Zhang, L. Zhang, H. Wu, M. Tian. Enhanced thermo-oxidative aging resistance of EPDM at high temperature by using synergistic antioxidants. Polym. Degrad. Stab. **102**, 1-8 (2014). https://doi.org/10.1016/j.polymdegradstab.2014.01.037

8. F. Cataldo. Early stages of p-phenylenediamine antiozonants reaction with ozone: Radical cation and nitroxyl radical formation. Polym. Degrad. Stab. **147**, 132-41 (2018). https://doi.org/10.1016/j.polymdegradstab.2017.11.020
9. F. Cataldo. Protection Mechanism of Rubbers from Ozone Attack. Ozone: Sci. Eng. **41**(4), 358-68 (2019). https://doi.org/10.1080/01919512.2018.1542518
10. J.C. Ambelang, R.H. Kline, O.M. Lorenz, C.R. Parks, C. Wadelin, J.R. Shelton. Antioxidants and Antiozonants for General Purpose Elastomers. Rubber Chem. Technol. **36**(5), 1497-541 (1963). https://doi.org/10.5254/1.3539652
11. Z. Tian, H. Zhao, K.T.Peter, M. Gonzalez, J. Wetzel, C. Wu, et al. A ubiquitous tire rubber–derived chemical induces acute mortality in coho salmon. Science. 371(6525), 185-9 (2021). 10.1126/science.abd6951
12. K. Hiki, K. Asahina, K. Kato, T. Yamagishi, R. Omagari, Y. Iwasaki, et al. Acute Toxicity of a Tire Rubber-Derived Chemical, 6PPD Quinone, to Freshwater Fish and Crustacean Species. Environ. Sci. Technol. Lett. **8**(9), 779-84 (2021). https://doi.org/10.1021/acs.estlett.1c00453
13. U. Hwang, B. Lee, B. Oh, H.S. Shin, S.S. Lee, S.G. Kang, et al. Hydrophobic lignin/polyurethane composite foam: An eco-friendly and easily reusable oil sorbent. Eur. Polym. J. **165**, 110971 (2022). https://doi.org/10.1016/j.eurpolymj.2021.110971
14. X. Pan, J.F. Kadla, K. Ehara, N. Gilkes, J.N. Saddler. Organosolv Ethanol Lignin from Hybrid Poplar as a Radical Scavenger: Relationship between Lignin Structure, Extraction Conditions, and Antioxidant Activity. J. Agric. Food Chem.. **54**(16), 5806-13 (2006). https://doi.org/10.1021/jf0605392
15. A. García, M.G. Alriols, G. Spigno, J. Labidi. Lignin as natural radical scavenger. Effect of the obtaining and purification processes on the antioxidant behaviour of lignin. Biochem. Eng. J. **67**, 173-85 (2012). https://doi.org/10.1016/j.bej.2012.06.013
16. U. Sukatta, P. Rugthaworn, W. Seangyen, R. Tantaterdtam, W. Smitthipong, R. Chollakup. Prospects for rambutan peel extract as natural antioxidant on the aging properties of vulcanized natural rubber. SPE Polymers. **2**(3), 199-209 (2021). https://doi.org/10.1002/pls2.10042
17. X. Lu, X. Gu, Y. Shi. A review on lignin antioxidants: Their sources, isolations, antioxidant activities and various applications. International Journal of Biological Macromolecules. **210**, 716-41 (2022). https://doi.org/10.1016/j.ijbiomac.2022.04.228
18. D.K. Setua, M.K. Shukla, V. Nigam, H. Singh, G.N. Mathur. Lignin reinforced rubber composites. Polym. Compos. **21**(6), 988-95 (2000). https://doi.org/10.1002/pc.10252
19. B. Košíková, A. Gregorová, A. Osvald, J. Krajčovičová. Role of lignin filler in stabilization of natural rubber–based composites. J. Appl. Polym. Sci. **103**(2), 1226-31 (2007). https://doi.org/10.1002/app.24530
20. R. Shorey, A. Gupta, T.H. Mekonnen. Hydrophobic modification of lignin for rubber composites. Ind. Crops Prod. **174**, 114189 (2021). https://doi.org/10.1016/j.indcrop.2021.114189
21. J. Liu, H.-F. Liu, L. Deng, B. Liao, Q.-X. Guo. Improving aging resistance and mechanical properties of waterborne polyurethanes modified by lignin amines. J. Appl. Polym. Sci. **130**(3), 1736-42 (2013).

https://doi.org/10.1002/app.39267

22. S. Lim, C.S. McArdell, U. von Gunten. Reactions of aliphatic amines with ozone: Kinetics and mechanisms. Water Res. **157**, 514-28 (2019). https://doi.org/10.1016/j.watres.2019.03.089
23. I.D.M. Figueredo, M.A.D.S. Rios, C.L. Cavalcante Jr, F.M.T. Luna. Effects of Amine and Phenolic Based Antioxidants on the Stability of Babassu Biodiesel Using Rancimat and Differential Scanning Calorimetry Techniques. Ind. Eng. Chem. Res. **59**(1), 18-24 (2020). https://doi.org/10.1021/acs.iecr.9b05209
24. C. Sirisinha, S. Phoowakeereewiwat, P. Saeoui. Cure and dynamic mechanical properties in peroxide-cured isoprene rubber: effects of stearic acid and amine-based antioxidant. Eur. Polym. J. **40**(8), 1779-85 (2004). https://doi.org/10.1016/j.eurpolymj.2004.03.002
25. A.Y. Coran. Chemistry of the vulcanization and protection of elastomers: A review of the achievements. J. Appl. Polym. Sci. **87**(1), 24-30 (2003). https://doi.org/10.1002/app.11659
26. C. Yang, Y. Luo, Z. Peng, K. Xu, J. Zhong. Comparison effects of lanthanum stearate and antioxidants in epoxidized natural rubber. J. Rare Earths. **33**(11), 1236-40 (2015). https://doi.org/10.1016/S1002-0721(14)60550-0
27. B.T. Poh BT, C.S. Te. Cure index and activation energy of vulcanization of natural rubber and epoxidized natural rubber vulcanized in the presence of antioxidants. J. Appl. Polym. Sci. **77**(14), 3234-8 (2000). https://doi.org/10.1002/1097-4628(20000929)77:14<3234::AID-APP270>3.0.CO;2-Q
28. Y. Sun, J. He, B. Zhong, L. Zhu, F. Liu. A synthesized multifunctional rubber additive and its improvements on the curing and antioxidative properties of styrene-butadiene rubber/silica composites. Polym. Degrad. Stab. **170**, 108999 (2019). https://doi.org/10.1016/j.polymdegradstab.2019.108999
29. X. Huang, G. Song, J. Shi, J. Ren, R.Guo, C. Li, G. Chen, Q. Li, Z. Zhou. Thermal stability, mechanical, and optical properties of novel RTV silicone rubbers using octa(dimethylethoxysiloxy)-POSS as a cross-linker. E-Polym. **22**(1), 357-369 (2022). https://doi.org/10.1515/epoly-2022-0022
30. X. Du, J. Li, M.E. Lindström. Modification of industrial softwood kraft lignin using Mannich reaction with and without phenolation pretreatment. Ind. Crops Prod. **52**, 729-35 (2014). https://doi.org/10.1016/j.indcrop.2013.11.035
31. X. Meng, B. Scheidemantle, M. Li, Y.-y. Wang, X. Zhao, M. Toro-González, et al. Synthesis, Characterization, and Utilization of a Lignin-Based Adsorbent for Effective Removal of Azo Dye from Aqueous Solution. ACS Omega. **5**(6), 2865-77 (2020). https://doi.org/10.1021/acsomega.9b03717
32. J. Chen, L. An, J.H. Bae, J.W. Heo, S.Y. Han, Y.S. Kim. Green and facile synthesis of aminated lignin-silver complex and its antibacterial activity. Ind. Crops Prod. **173**, 114102 (2021). https://doi.org/10.1016/j.indcrop.2021.114102
33. M.N.M. Ibrahim, N. Zakaria, C.S. Sipaut, O. Sulaiman, R. Hashim. Chemical and thermal properties of lignins from oil palm biomass as a substitute for phenol in a phenol formaldehyde resin production. Carbohydr. Polym. **86**(1), 112-9 (2011). https://doi.org/10.1016/j.carbpol.2011.04.018

34. S. Bhagia, J. Ďurkovič, R. Lagaňa, M. Kardošová, F. Kačík, A. Cernescu, P. Schäfer, C G. Yoo, AJ. Ragauskas. Nanoscale FTIR and Mechanical Mapping of Plant Cell Walls for Understanding Biomass Deconstruction. ACS. Sustain. Chem. Eng. **10**(9), 3016-3026 (2022). https://doi.org/10.1021/acssuschemeng.1c08163
35. G.-J. Jiao, P. Peng, S.-L. Sun, Z.-C. Geng, D. She. Amination of biorefinery technical lignin by Mannich reaction for preparing highly efficient nitrogen fertilizer. Int. J. Biol. Macromol. **127**, 544-54 (2019). https://doi.org/10.1016/j.ijbiomac.2019.01.076
36. S. Nikafshar, O. Zabihi, Y. Moradi, M. Ahmadi, S. Amiri, M. Naebe. Catalyzed Synthesis and Characterization of a Novel Lignin-Based Curing Agent for the Curing of High-Performance Epoxy Resin. Polymers. **9**(7), 266 (2017). https://doi.org/10.3390/polym9070266
37. H. Pan, G. Sun, T. Zhao. Synthesis and characterization of aminated lignin. Int. J. Biol. Macromol. **59**, 221-6 (2013). https://doi.org/10.1016/j.ijbiomac.2013.04.049
38. R. Seenu, S. Zhang, Y.-R. Lee, K.-K. Kang, J.-M. Kim, J.-W. Ahn, et al. EDTA-functionalized KCC-1 and KIT-6 mesoporous silicas for Nd 3+ ion recovery from aqueous solutions. J. Ind. Eng. Chem. **67**, 210-218 (2018). https://doi.org/10.1016/j.jiec.2018.06.031
39. M. Wysokowski, Ł. Klapiszewski, D. Moszyński, P. Bartczak, T. Szatkowski, I. Majchrzak, K. Siwińska-Stefańska, VV. Bazhenov, T. Jesionowski. Catalyzed Modification of Chitin with Kraft Lignin and Development of New Biosorbents for Removal of Cadmium(II) and Nickel(II) Ions. Mar. Drugs. **12**(4), 2245-2268 (2014). https://doi.org/10.3390/md12042245
40. Q. Yan, R. Arango, J. Li, Z. Cai. Fabrication and characterization of carbon foams using 100% Kraft lignin. Mater. Des. **201**, 109460 (2021). https://doi.org/10.1016/j.matdes.2021.109460
41. H. Wang, W. Liu, J. Huang, D. Yang, X. Qiu. Bioinspired Engineering towards Tailoring Advanced Lignin/Rubber Elastomers. Polymers. **10**(9), 1033 (2018). https://doi.org/10.3390/polym10091033
42. Y. Ikeda, T. Phakkeeree, P. Junkong, H. Yokohama, P. Phinyocheep, R. Kitano, et al. Reinforcing biofiller “Lignin” for high performance green natural rubber nanocomposites. RSC Adv. **7**(9), 5222-31 (2017). 10.1039/C6RA26359C
43. Y. Zhang, N.G. Pavlopoulos, T.S. Kleine, M. Karayilan, R.S. Glass, K. Char, et al. Nucleophilic Activation of Elemental Sulfur for Inverse Vulcanization and Dynamic Covalent Polymerizations. J. Polym. Sci. A. Polym. Chem. **57**(1), 7-12 (2019). https://doi.org/10.1002/pola.29266
44. J.W. Thomson, K. Nagashima, P.M. Macdonald, G.A. Ozin. From Sulfur–Amine Solutions to Metal Sulfide Nanocrystals: Peering into the Oleylamine–Sulfur Black Box. J. Am. Chem. Soc. **133**(13), 5036-41 (2011). https://doi.org/10.1021/ja1109997
45. E. Manaila, M.D. Stelescu, G. Craciun. Degradation Studies Realized on Natural Rubber and Plasticized Potato Starch Based Eco-Composites Obtained by Peroxide Cross-Linking. Int. J. Mol. Sci. **19**(10), 2862 (2018). https://doi.org/10.3390/ijms19102862
46. D.D. Jiang, G.F. Levchik, S.V. Levchik, C.A. Wilkie. Thermal decomposition of cross-linked polybutadiene and its copolymers. Polym. Degrad. Stab. **65**(3), 387-94 (1999). https://doi.org/10.1016/S0141-3910(99)00027-0

47. N. Dehbari, Y. Tang. Water swellable rubber composites: An update review from preparation to properties. J. Appl. Polym. Sci. **132**, 46 (2015). https://doi.org/10.1002/app.42786
48. L.R. Evans, D.A. Benko, J.G. Gillick, W.H. Waddell. Microencapsulated Antidegradants for Extending Rubber Lifetime. Rubber Chem. Technol. **65**(1), 201-10 (1992). https://doi.org/10.5254/1.3538600
49. F. Ignatz-Hoover, B.H. To, R.N. Datta, A.J. De Hoog, N.M. Huntink, A.G. Talma. Chemical Additives Migration in Rubber. Rubber Chem. Technol. **76**(3), 747-68 (2003). https://doi.org/10.5254/1.3547765
50. G. Weng, G. Huang, H. Lei, L. Qu, Y. Nie, J. Wu. Crack initiation and evolution in vulcanized natural rubber under high temperature fatigue. Polym. Degrad. Stab. **96**(12), 2221-8 (2011). https://doi.org/10.1016/j.polymdegradstab.2011.09.004
51. Z. Wang. Research on fatigue failure mode and failure theory of rubber. J. Phys. Conf. Ser. **2076**(1), 012079 (2021). https://doi.org/10.1088/1742-6596/2076/1/012079

Figures

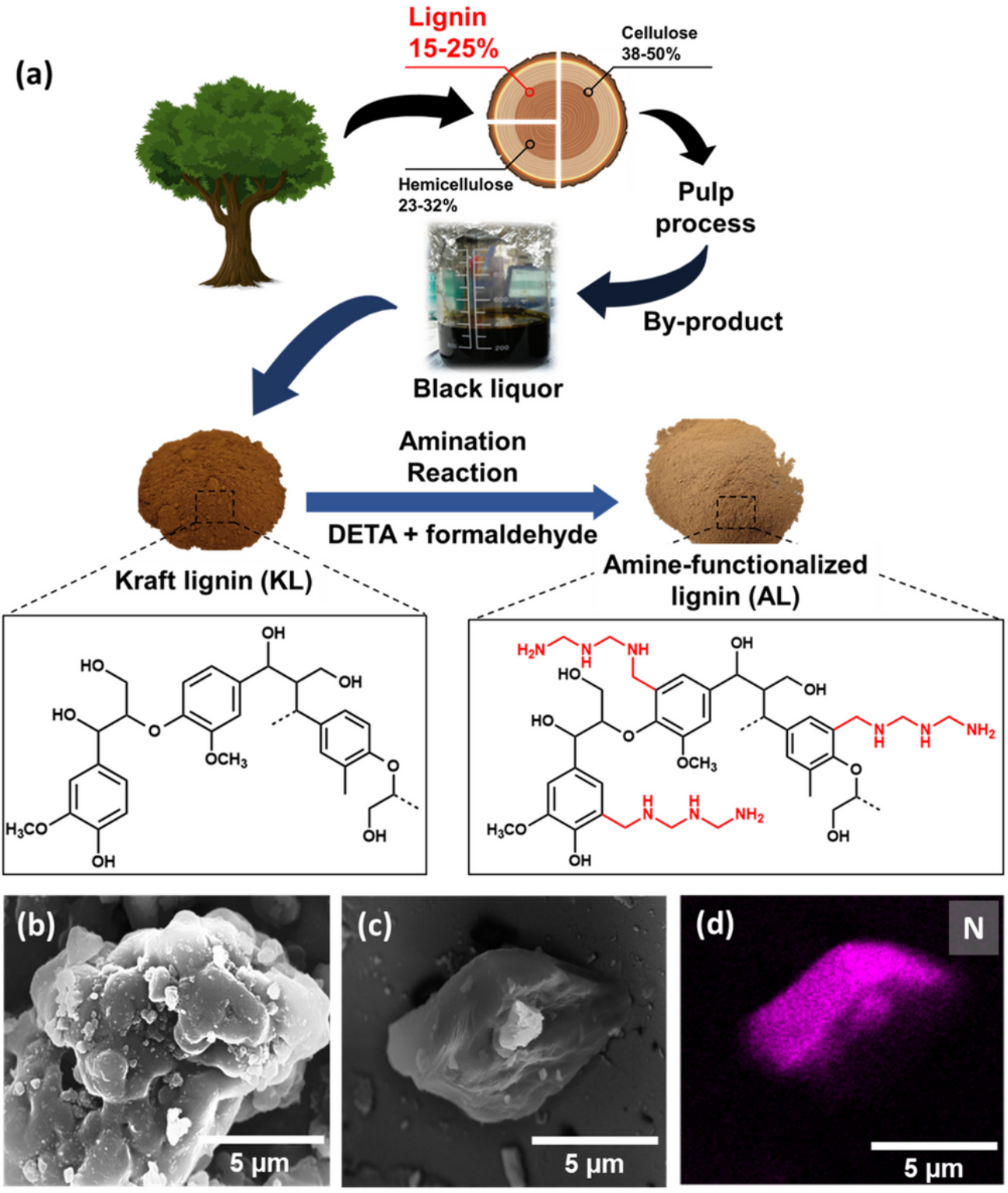

Figure 1

(a) Schematic illustration of the process used to fabricate AL via the amination reaction. FE-SEM images of (b) KL and (c) AL particles with (d) corresponding EDS elemental N mapping image.

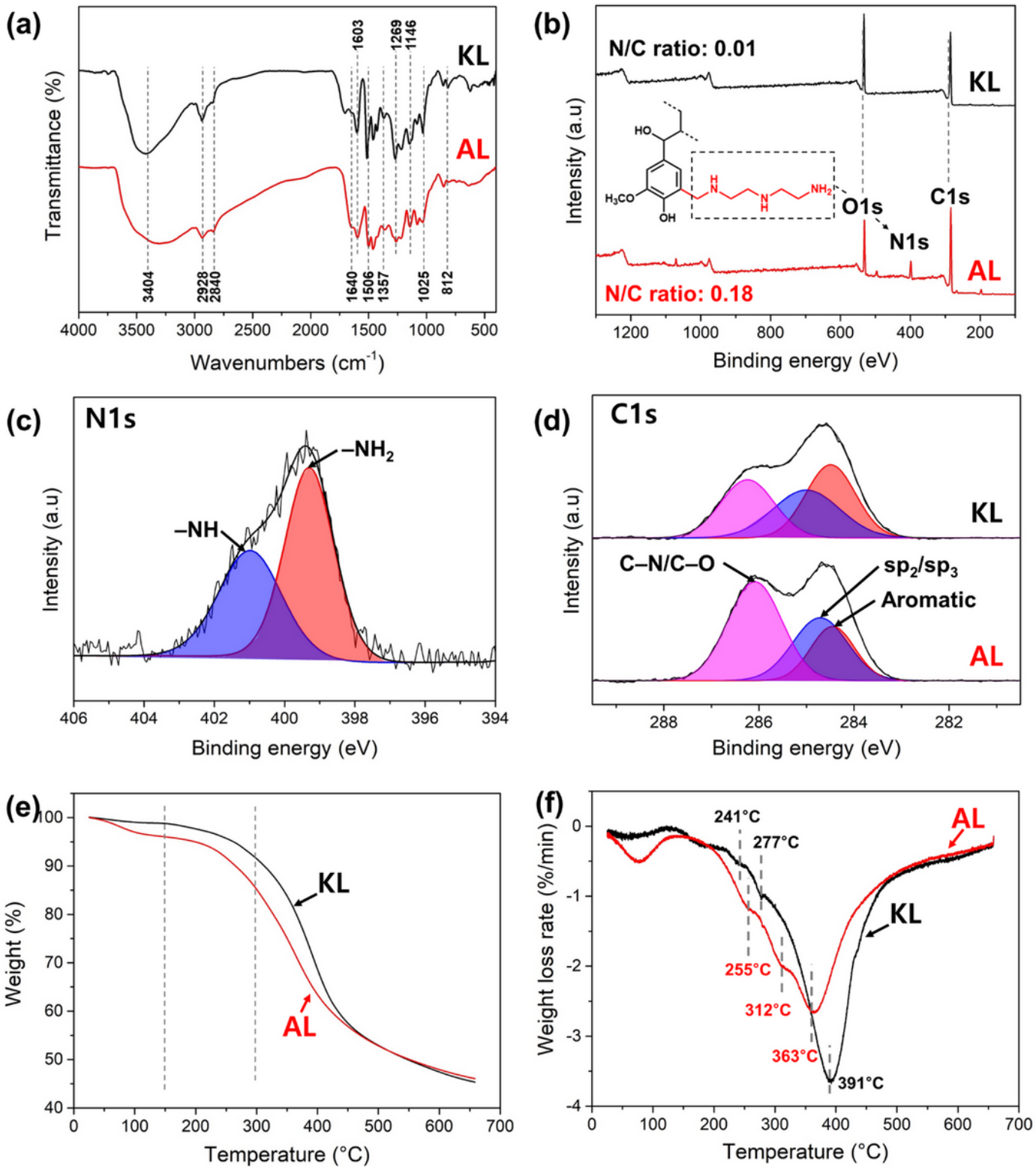

Figure 2

Comparative spectral analyses of KL and AL: (a) FT-IR spectra, (b) XPS wide-scan spectra (inset: chemical structure of AL), (c) XPS N1s core-level spectra of AL, and (d) XPS C1s core-level spectra of KL and AL. (e) TGA and (f) DTG thermograms of KL and AL obtained under N_2 atmosphere.

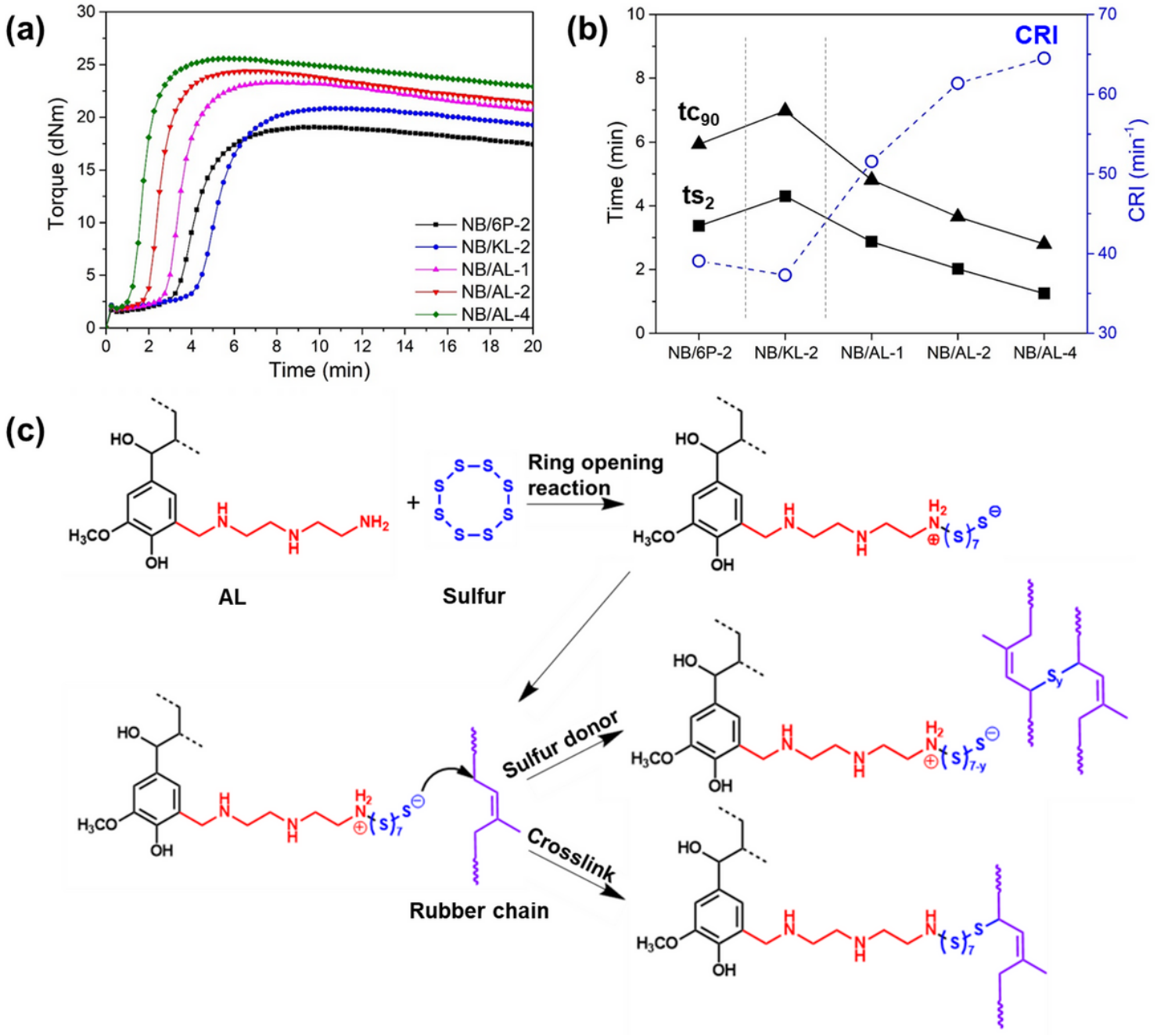

Figure 3

Rheological properties of rubber compounds added with different antioxidants at 160 °C: (a) torque as a function of time, (b) curing time (ts_2 and tc_{90}) and CRI. (c) Expected mechanisms of the heterolytic ring-opening reaction between AL and sulfur, and subsequent rubber crosslinking reaction.

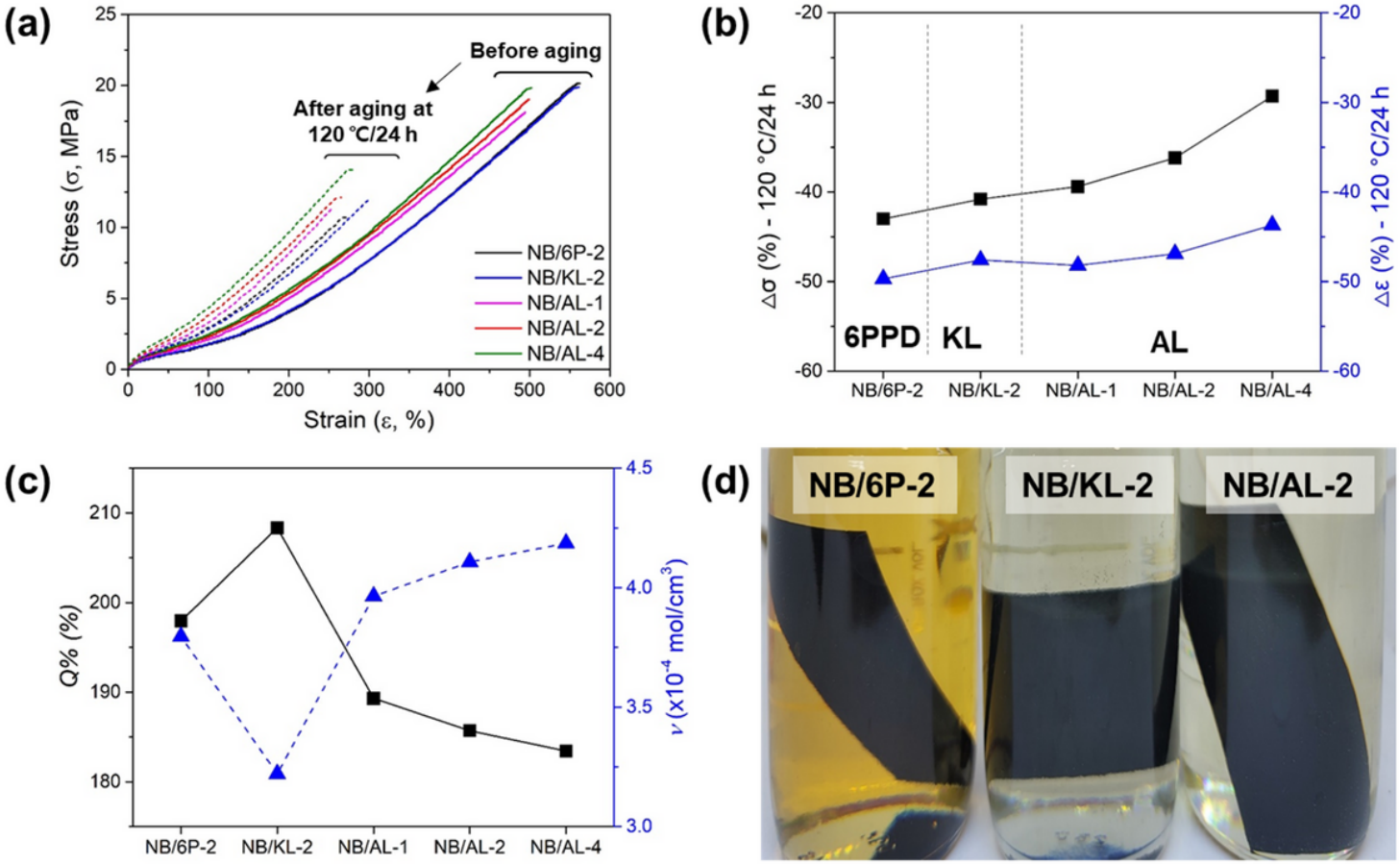

Figure 4

Tensile properties of rubber compounds in terms of antioxidant content and thermal aging: (a) stress–strain curves obtained before aging and after aging at 120 °C for 24 h and (b) degradation of the tensile strength and elongation. (c) Degree of swelling and crosslink density of NB compounds and (d) corresponding digital images of the samples in solvent after 48 h.

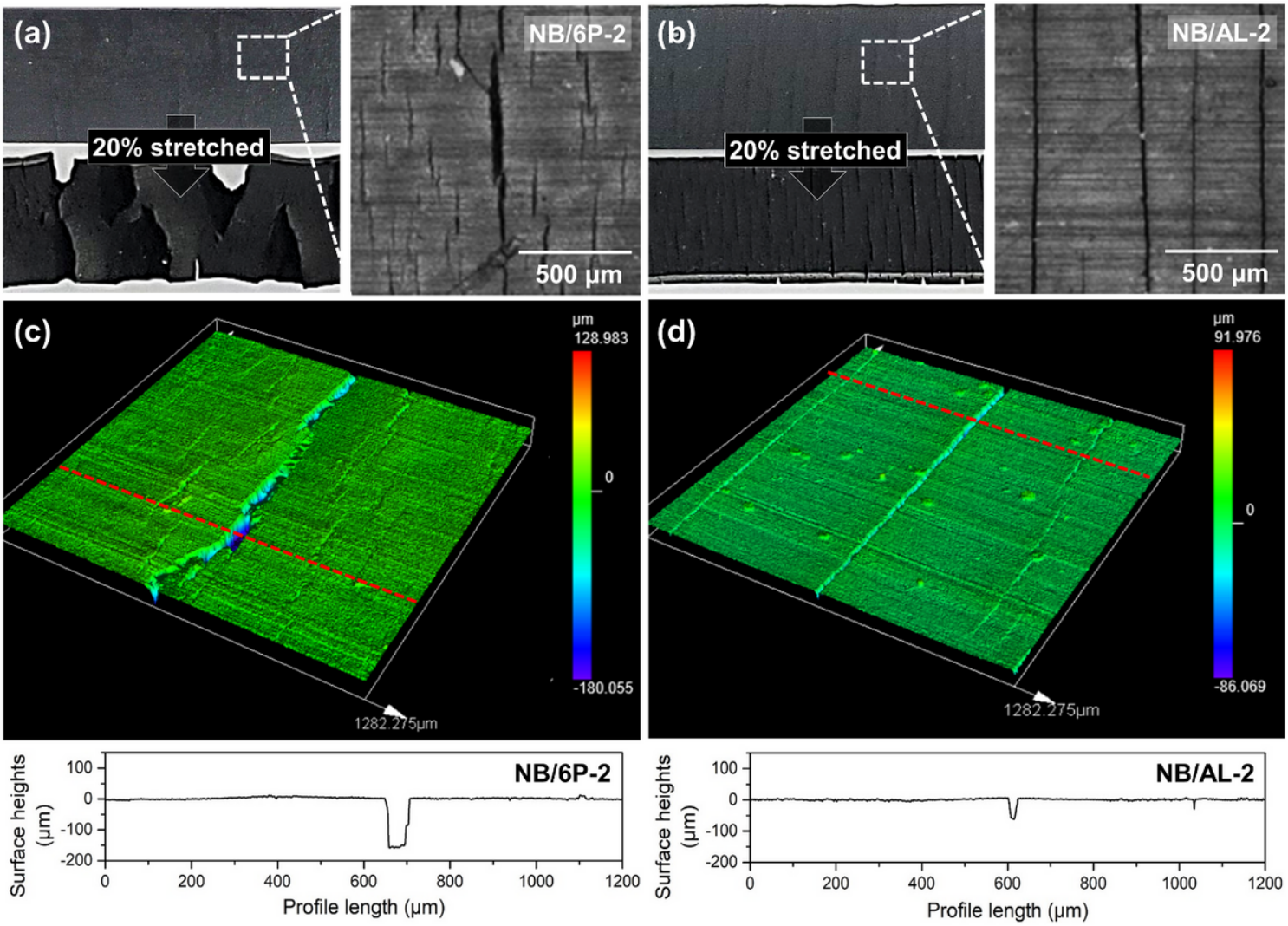

Figure 5

Digital images of ozone-aged (a) NB/6P-2 and (b) NB/AL-2 at a strain of 0 and 20%, respectively, and corresponding optical microscope images. 3D LSM images of (c) NB/6P-2 and (d) NB/AL-2 with corresponding surface profile extracted over dotted red lines.

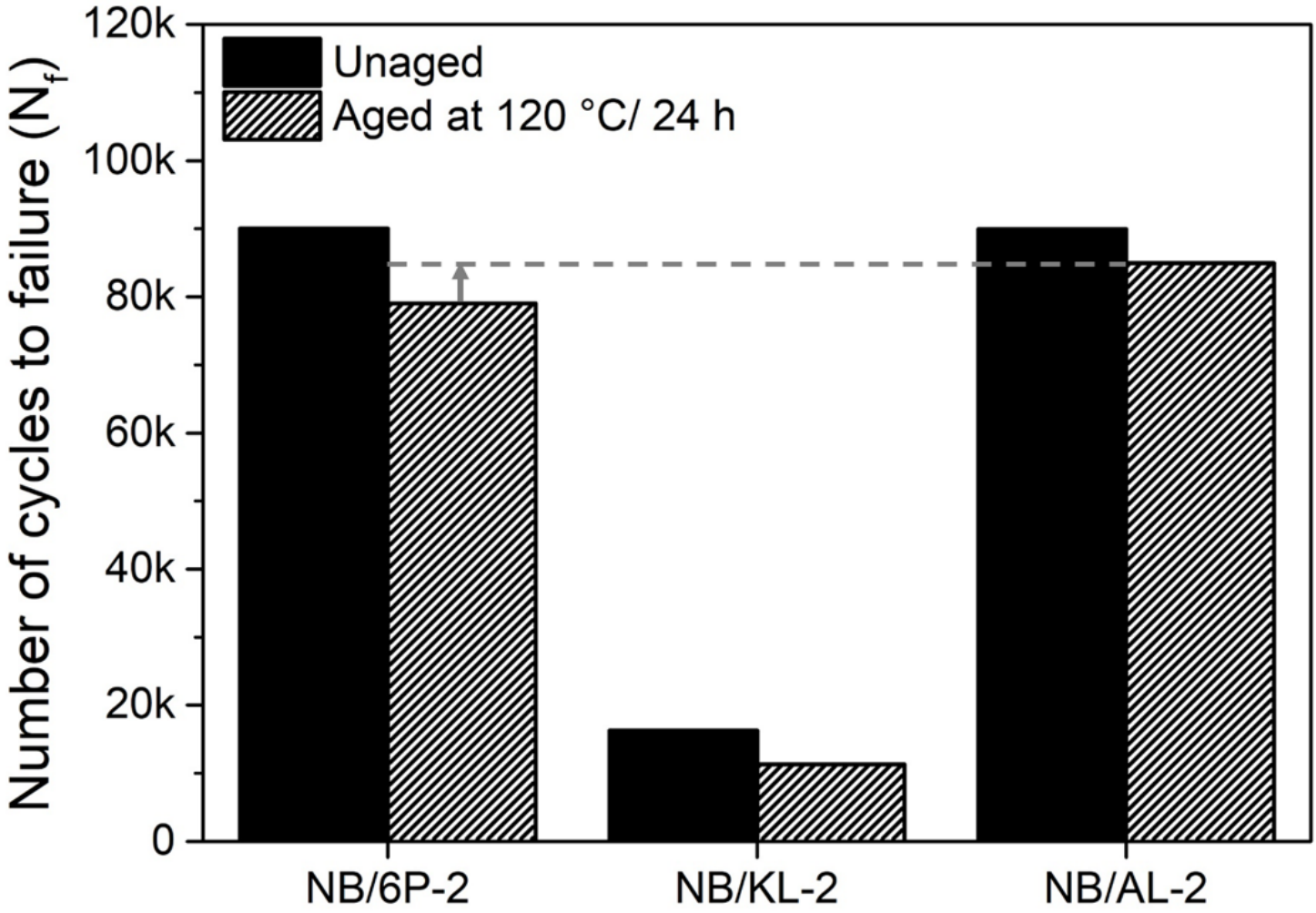

Figure 6

Number of cycles to failure of NB compounds comparing the fatigue resistances of unaged and thermally aged samples (at 120 °C for 24 h).

Supplementary Files

This is a list of supplementary files associated with this preprint. Click to download.

- SupplementaryMaterialALACHM.docx
- GA.png